WIDE RANGE TUNING OF SLOW LIGHT PULSE IN SOI PHOTONIC CRYSTAL COUPLED WAVEGUIDE VIA FOLDED CHIRPING

Jun Adachi, Norihiro Ishikura, Hirokazu Sasaki, and Toshihiko Baba, *Member, IEEE*

(Invited Paper)

***Abstract*— We demonstrate state-of-the-art slow light in silicon-on-insulator photonic crystal coupled waveguide, which allows slow light pulse transmission and its tunable delay by means of structural chirping. The key idea of this study is the application of a folded chirping profile to the structure, instead of the conventional monotonous chirping. It suppresses unwanted spectral oscillation caused by structural disordering and expands the tuning range. By post-processing an airhole-diameter- chirped device, we show that 0.9-ps-wide slow light pulses are delayed for 72 ps, corresponding to a buffering capacity of 80 bits. In a separate, unchirped device, we demonstrate a tunable delay by applying thermally induced index chirping. Here, a maximum tuning range of 103 ps and tunable capacity of 22 bits are obtained.**

***Index Terms*— photonic crystal, photonic crystal waveguide, slow light, optical buffer, delay line**

I. INTRODUCTION

Slow light with a markedly low group velocity provides a long and tunable delay (in other words, effective and variable interaction with materials) in a compact device [1, 2]. Therefore, it is anticipated to achieve optical buffering, time-domain optical signal processing, and enhancement of linear/nonlinear effects. Photonic nanostructures, e.g. photonic crystals (PCs) and microring resonators, are studied extensively toward on-chip slow light devices compatible to advanced photonic integrated circuits such as silicon photonics [3-12]. For this purpose, we have proposed chirped photonic crystal coupled waveguide (PCCW) as a promising device, and have demonstrated this on a PC slab platform fabricated into silicon-on-insulator (SOI) substrate [13-16]. It clears two crucial issues of slow light: wide bandwidth and low group velocity dispersion (GVD). An optimum PCCW exhibits a photonic band of guided mode suitable for slow light generation as well as internal GVD compensation. The chirping formed by linearly changing structural parameters along the waveguide arbitrarily expands the bandwidth in proportion to the chirp range. So far, we designed and fabricated devices in which chirping was formed to the airhole diameter of the PC slab. We observed a bandwidth of wider than 1 THz and low GVD for slow light, which allow short, picosecond pulses to slow down. In addition, we demonstrated that the delay of the slow light pulses can be controlled externally by sloped laser heating. In a PCCW of 250 μm length, a delay of approximately 40 ps and a tuning range of 23 ps were obtained for pulses with an width of 3.3 ps, corresponding to buffering and tunable capacities of 12 and 6 bits, respectively.

The present paper discusses the enhancement of these values. Two simple ways for this are to elongate the device and improve the heating efficiency. However, in longer devices the slow light characteristics become more sensitive to structural disordering. When the device is elongated without changing the chirp range, in order to achieve the same target bandwidth, the chirp slope is reduced and the disordering could locally invert the chirp direction. It gives rise to unwanted mode gaps and internal resonance around the slow light areas, resulting in large oscillation of transmission and delay spectra, as well as the local GVD. In this paper, we propose folded chirping, in which the direction of the chirping is intentionally inverted at positions not overlapping with slow light areas. It is advantageous because it gives the same delay for a larger chirp slope, suppressing the influence of the disordering. It is also effective for expanding the tuning range by the laser heating.

This paper is structured as follows. Section II outlines the structural details and expected operation of the folded-chirped PCCW. Section III summarizes the fabrication method of SOI-based devices and experimental setups for measuring the slow light characteristics and the application of thermal tuning by laser heating. Then, Section IV presents experimental results for a device in which the airhole diameter is chirped. Here we demonstrate that the slow light spectra are improved by the folded chirping, and a large buffering capacity is confirmed for slow light pulses when the device is heated to adjust the internal GVD compensation. Section V presents the results of a device without the airhole diameter chirping. First, we show slow light spectra obtained by post-processing, where the folded chirp is

Manuscript received May 1, 2009. (Write the date on which you submitted your paper for review.)

Authors are with the Department of Electrical and Computer Engineering, Yokohama National University, 79-5 Tokiwadai, Hodogaya-ku, Yokohama 240-8501, Japan (corresponding author to provide phone: +81-45-339-4258; fax: +81-45-338-1157; e-mail: baba@ynu.ac.jp).

J. Adachi, S. Sasaki and T. Baba are also with CREST, Japan Science and Technology Agency, 5 Sanbancho, Chiyoda-ku, Tokyo 102-0075, Japan

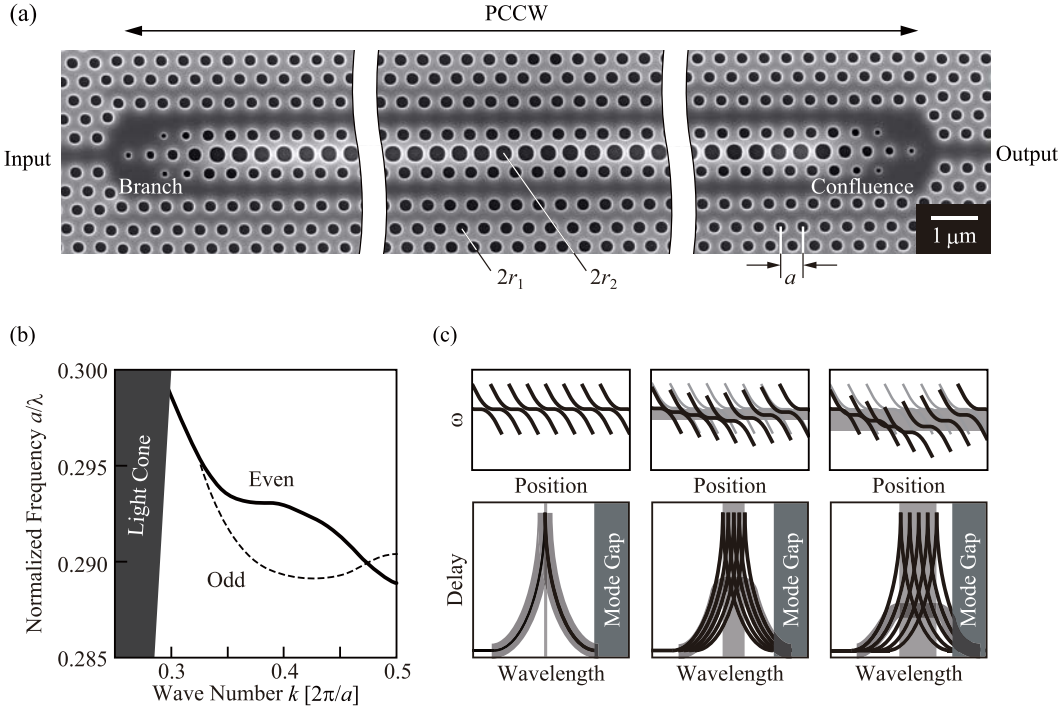

Fig. 1. Structure and expected characteristics of PCCW. (a) Top view of fabricated device on SOI substrate. (b) Calculated photonic band diagram of even and odd symmetric guided modes. (c) Schematics of position-dependent band curve of the even symmetric mode (upper figures) and group delay spectrum (lower figures) in the device with folded chirping. Three figures assume different chirp ranges. In the lower figures, thin black lines show the delay spectra at each position, and thick gray lines the delay spectrum averaged by the chirping.

induced purely by heating. Then, by varying the extent of heating, we report record wide range tuning of the pulse delay.

II. Structure and Principle

Fig. 1(a) shows the PCCW fabricated on a SOI substrate with a top Si layer of 0.22 μm thickness. The PC slab consists of an airbridge Si slab with triangular lattice circular airholes. The PCCW consists of two parallel line defect waveguides separated by three rows of airholes. It is connected to input and output waveguides through symmetric branch and confluence, which are optimized for lowering loss [15]. These waveguides are sandwiched by a pair of PC claddings, each consisting of 14 rows of airholes. To achieve efficient heating mentioned later, the PCCW is thermally insulated from outer areas by a series of rectangular airholes each separated by 1-μm-wide beams. The lattice constant a and default airhole diameter $2r_1$ of the PC are set at 0.46 μm and 0.25 μm, respectively, so that slow light is generated at wavelengths around $\lambda \approx 1.55$ μm. For the fine tuning of the photonic band shape, the diameter of the central row of airholes, $2r_2$, is enlarged to 0.36 μm, while each row just outside of the two line defects of the PCCW is shifted towards the center by 0.1 μm. The photonic band is calculated using three-dimensional finite-difference time-domain (FDTD) method with periodic boundary condition, assuming the refractive indices of Si and air to be 3.5 and 1.0, respectively, as shown in Fig. 1(b). Even and odd symmetric guided modes appear for the transverse-electric-like polarization. Only the even symmetric mode is excited in the PCCW when the branch is symmetric. Here, this mode exhibits an ideal flat band with an inflection point sandwiched by opposite GVD characteristics. A long delay is expected at the flat-band frequency due to its zero group velocity. When the band is frequency-shifted by structural chirping, wideband dispersion-compensated slow light is obtained because each wavelength component passes through the slow light area as well as the two opposite GVD areas as well. When $2r_1$ is shifted from 0.25 to 0.27 μm for the above-mentioned device design, the slow light band extends from $\lambda = 1.548$ to 1.560 μm [16].

In such chirped structures, photonic bands simply frequency-shift while retaining its shape, as long as the total amount of the chirping is small. The average group index $\tilde{n}_g$ is given by [14]

$$\tilde{n}_g = \frac{c\Delta t}{L} = c\frac{\Delta k}{\Delta \omega} \tag{1}$$

where Δt and $\Delta\omega$ are the delay and bandwidth of slow light, respectively, Δk is the change in propagation constant due to the chirping, L is the length of the PCCW, and c is the vacuum velocity of light. The delay-bandwidth product is a crucial measure for potential buffering capacity of slow light. For chirped structures, it is given by

$$\Delta t \Delta f = L\frac{\Delta k}{2\pi} = \Delta n \frac{L}{\lambda} \tag{2}$$

where $\Delta f = \Delta\omega/2\pi$ and Δn is the change in modal equivalent index given by $\Delta k = \Delta n(2\pi/\lambda)$. Eq. (2) is absolutely the same as

the general formulas for slow light, and depicts that the delay is constrained by the bandwidth even in chirped structures. Here, Δn is determined by the original band shape and the amount of chirping. Eq. (2) suggests that the same delay is expected for the same amount of the chirping, regardless of the chirp profile.

In previous studies, we have employed monotonous chirping of the airhole diameter $2r_1$ and slab index in the PCCW, and demonstrated slow light pulses with tunable delay. In contrast, in this study we discuss the notion of *folded* chirping, in which the chirp direction is reversed at the device center, as illustrated in Fig. 1(c). It is advantageous for both the airhole diameter and index chirping, compared with the monotonous chirping. In our experiment, airhole diameters have a typical rms error of ±1.5 nm from ideal values of the chirping. This disordering cannot be ignored against the total chirp range of 20 nm for the above design, and causes large spectral oscillation for a small chirp slope in longer devices. But the folded chirping keeping a large chirp slope can suppress this oscillation. The index chirping can be tuned through external control such as heating, carrier injection, and applied electric field. Here we exploit the thermo-optic effect by laser heating, in which a blue-violet laser spot is irradiated from above the device. Due to the thermal insulation of the large, rectangular airholes, a large index change of the order of 10^{-2} is easily obtained. To induce a monotonous index chirp, the laser spot is centered on one end of the PCCW, such that one half of the laser spot irradiates the PCCW, while the other half irradiates an area that does not affect the PCCW. Since the spot intensity decreases from one end of the PCCW to the other, a monotonous chirp is formed. In contrast, the folded chirp is formed easily by irradiating the whole laser spot around the device center, so that the spot intensity and hence the thermo-optic index change decreases away from the center. This doubles the chirp length and tuning range with the same heating power.

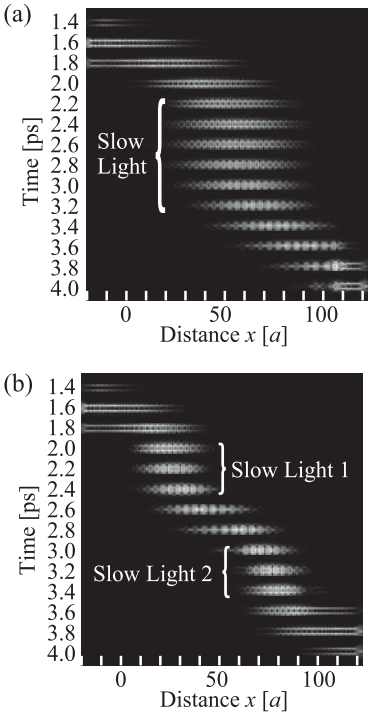

Fig. 2. FDTD simulation of slow light pulse propagation in PCCW. (a) Monotonous chirping. (b) Folded chirping.

Fig. 2 shows the FDTD simulation of a slow light pulse propagating through the PCCW with the two chirp profiles. To save the computation time, we used the two-dimensional approximation. Therefore, structural parameters in this calculation are modified from those described above such that $2r_1 = 0.59a$ and $2r_2 = 0.20a$ with a device length $L = 125a$. The chirping is assumed only for the equivalent slab index from 2.870 to 2.963 to model sufficiently smooth chirping. The detail of the computation conditions is the same as that presented previously [13]. In the case of monotonous chirping, the light pulse temporally stops only once as it propagates through the PCCW. In the case of the folded chirp, the same thing occurs, but it occurs twice. It occurs once in each half of the PCCW, and with half the stopping time of the monotonous case. Therefore, the total delay is kept constant between the two cases. This result supports the above discussion that Eq. (2) is preserved for both chirp profiles.

III. Methods

In the experiment, we used smart-cut SOI substrate, obtained from SOITEC. The top Si layer and SiO_2 box layer were 0.21 μm and 2.0 μm thick, respectively. The airhole pattern of the PC slab was formed using *e*-beam writer Elionix ELS7500EX, with 50 keV field-emission gun, and *e*-beam resist Zeon ZEP520a, with 0.4 μm thickness after spin coating. The field size was 300 or 600 μm and resolved by 60,000 dots. The airholes were perforated into the Si layer through the resist mask using inductively coupled plasma etcher SAMCO RIE-10ip with SF_6 gas. After removing the resist and lapping the substrate to less than 100 μm, the substrate is cleaved to form two waveguide facets. Finally, the airbridge structure was formed by HF wet etching of the box layer. We fabricated the devices with and without folded chirping of the diameter $2r_1$. To form smooth chirping, the exposure time of the *e*-beam writing was gradually changed for the same designed diameter. Specifications of the *e*-beam writer only ensure a resolution of the exposure time, which forms a six-level step-like chirp profile in the chirp range of 20 nm. However, the airhole diameter measured shows a much smoother profile [16], suggesting a higher effective resolution. The chirp range is reproducible, while the absolute airhole diameter fluctuates between samples. A 10 nm increase in $2r_1$ leads a wavelength blueshift of 13 nm. Therefore, we fabricate many samples and pick up some of them, which are suitable for measurement setups described below. In the unchirped device, it is particularly important to adjust $2r_2$ precisely, in order to achieve an ideal flat band. To achieve this, we measured the group delay spectrum after fabrication and repeated a

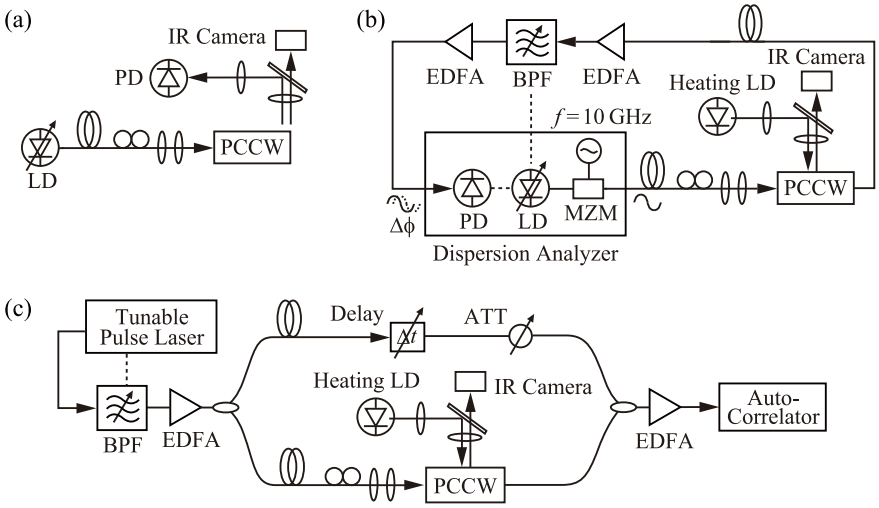

Fig. 3. Measurement setups for (a) transmission spectrum, (b) group delay spectrum using modulation phase shift method, and (c) pulse transmission.

post-process consisting of O_2 plasma irradiation and HF etching, so that a sharp delay peak at the flat band was obtained.

Fig. 3 shows three setups for measuring the slow light characteristics. In all of them, TE polarized incident light was focused to a ~1 μm diameter spot using objective lenses and coupled to the waveguide facet. Output light from the other facet was detected from above the device through another objective lens or from the lateral direction using lensed fiber. The transmission spectrum was simply measured using tunable laser and power meter. As shown in Fig. 3(a), although its detection efficiency is lower, we used the first detection scheme, because it is effective for eliminating the direct coupling of incident light and assuring a large dynamic range of the spectrum. The group delay spectrum was measured using modulation phase shift method with the second detection scheme to acquire a higher detection efficiency, as shown in Fig. 3(b). In this measurement, tunable laser light is modulated at a frequency f_m of 10 GHz and transmitted through the device. The delay Δt is evaluated from the relation $\Delta\phi = 2\pi f_m \Delta t$, where $\Delta\phi$ is the phase shift between the input and output facets. Erbium-doped fiber amplifier (EDFA) was used to compensate the insertion loss of the device of more than 30 dB (primarily coupling loss with the external setup). Amplified spontaneous emission noise of the EDFA was eliminated by tunable band pass filter (BPF). The second EDFA was inserted before phase detection to further improve the signal-to-noise ratio. The pulse transmission was measured using tunable passively mode-locked fiber laser, as shown in (c). Spectrum of the laser pulse was appropriately narrowed using wavelength- and bandwidth-tunable BPF. It was then amplified by EDFA and branched into two by a fiber coupler. One was inserted into the device and the other was passed through mechanically tunable delay line and attenuator as a reference. They were combined by the second coupler, amplified by the second EDFA and evaluated by autocorrelator. The autocorrelation of the reference pulse appears at a reference time. The cross-correlation between the reference pulse and the pulse passing through the device shows the delay against the reference time. Approximating the pulse shape to be Gaussian, the full-width at half-maximum (FWHM) of the reference pulse $\Delta\tau_{ref}$ is evaluated using the relation $\Delta\tau_{mes}^2 = 2\Delta\tau_{ref}^2$ for the FWHM of measured trace $\Delta\tau_{mes}$. The FWHM of the output pulse from the device $\Delta\tau_o$ is evaluated using the relation $\Delta\tau_{mes}^2 = \Delta\tau_o^2 + \Delta\tau_{ref}^2$.

For the laser heating, high-power blue-violet laser diode at $\lambda = 0.442$ μm was used to enhance the absorption efficiency in the Si layer. The laser spot was deformed to an elliptical profile (400×180 μm^2) by using cylindrical and objective lenses. The spot was irradiated to the center of the device in most results shown below, while moved to optimum positions in the last result.

IV. Device with Airhole Diameter Chirping

Fig. 4(a) and (b) show the transmission and delay spectra for monotonous and folded chirping of the airhole diameter. The length of the PCCW was 400 μm and $2r_1$ was chirped from 0.25 μm at the branch to 0.26μm toward the confluence. For both chirping, the transmission intensity drops at the cutoff of the waveguide mode on the long wavelength side. The delay spectrum indicates that a long delay Δt due to slow light occurs in a wavelength bandwidth of 10 nm on the shorter wavelength side of the cutoff. Note that the transmission intensity in the slow light regime is not necessarily weaker than that in the fast light regime. Similar results are often observed in chirped slow light devices [15, 16]. It is quite a contrast to the case that scattering loss caused by the disordering is noticeably enhanced with slow light in unchirped structures, as shown later. Reason for this is not clear, but it might be due to an effect that the correlation length of scattered waves is particularly shortened

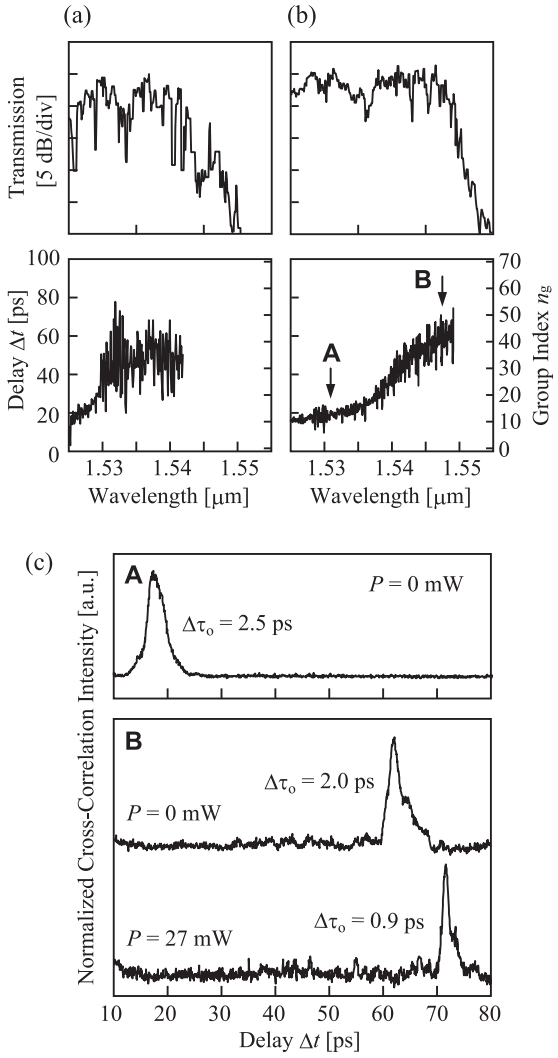

Fig. 4. Slow light characteristics of 400-μm-long chirped PCCW. (a) Transmission and delay spectra of monotonous- chirped device, and (b) those of folded-chirped device. (c) Normalized cross-correlation trace of output pulse, where **A** and **B** correspond to those in (b).

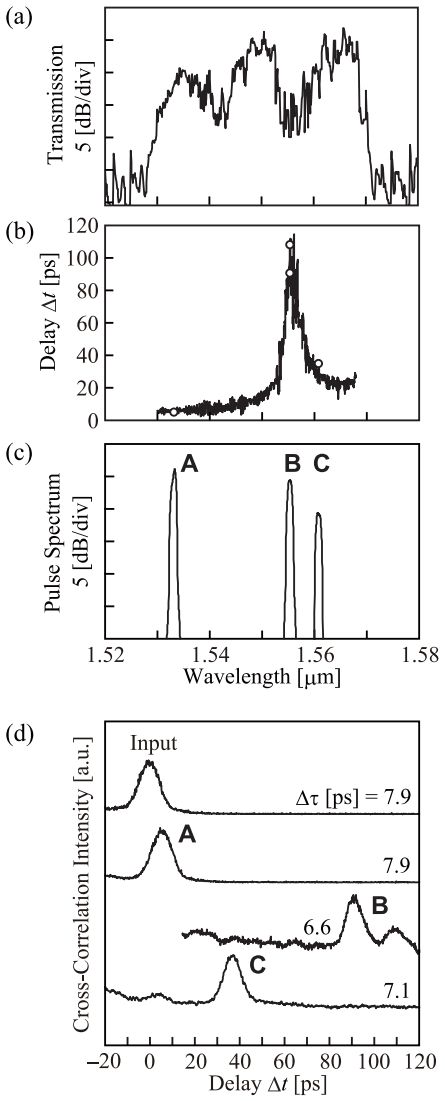

Fig. 5. Slow light characteristics of 280-μm-long unchirped PCCW. (a) Transmission spectrum. (b) Delay spectrum. (c) Spectrum of incident pulse. (d) Normalized cross-correlation trace of output pulse, where **A** - **C** correspond to those in (c).

in chirped structures and the multi-scattering process [17, 18] is suppressed. Let us compare the results for two different chirping. The folded chirping exhibits a 2 – 3 dB higher transmission intensity with smaller oscillation than those of the monotonous chirping. Accordingly, the delay increased with smaller oscillation. These are the evidence that the influence of the disordering was reduced by the larger chirp slope of the folded chirping.

Fig. 4(c) shows the cross-correlation trace of output pulse for the folded chirping, where $\Delta\tau_{ref}$ = 0.9 ps and the corresponding wavelength width (FWHM) $\Delta\lambda_{3dB}$ restricted by the BPF was 2.0 nm. The output pulse was clearly observed at both fast and slow light wavelengths, and the delay of the pulse center was in good agreement with those in Fig. 4(b). Compared with the reference pulse, the output pulse in both fast and slow light regimes was slightly dispersed as $\Delta\tau_o$ = 2.5 and 2.0 ps, respectively. The larger dispersion in the fast light regime might be due to the small GVD at frequencies above the slow light one. Then we performed the laser heating for the folded chirping. The delay increased as the index chirping partially cancels the airhole diameter chirping. Note that the pulse width narrowed with the heating. We observed similar behaviors in many samples. A reasonable explanation for this result is as follows. The opposite GVD characteristics of the PCCW are not perfectly symmetric about the inflection point of the photonic band. Also, the index chirping profile depends on the laser spot profile and thermal diffusion, and is not perfectly linear. The former imperfection could be compensated by the latter. Here, the pulse of 0.9 ps width was delayed for 72 ps. These values ensure a fractional delay $\Delta t/\Delta\tau_o$ of 80, which is equivalent to a net buffering capacity.

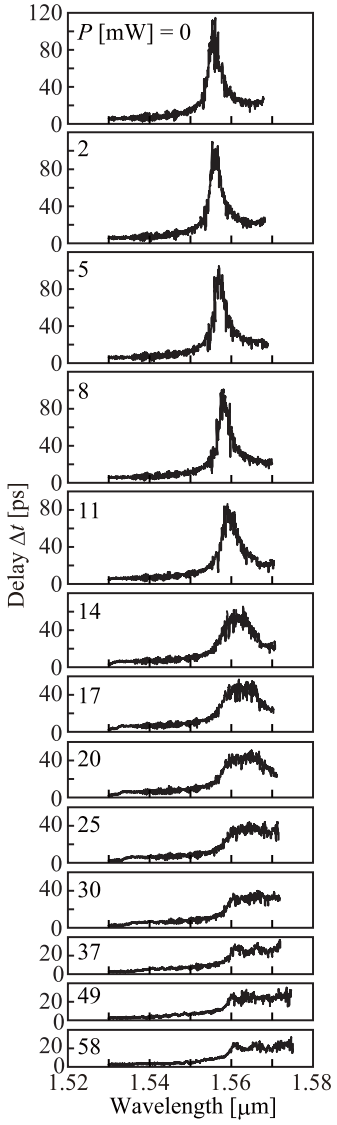

Fig. 6. Change of the delay spectrum with the heating power in the same device as for Fig. 5.

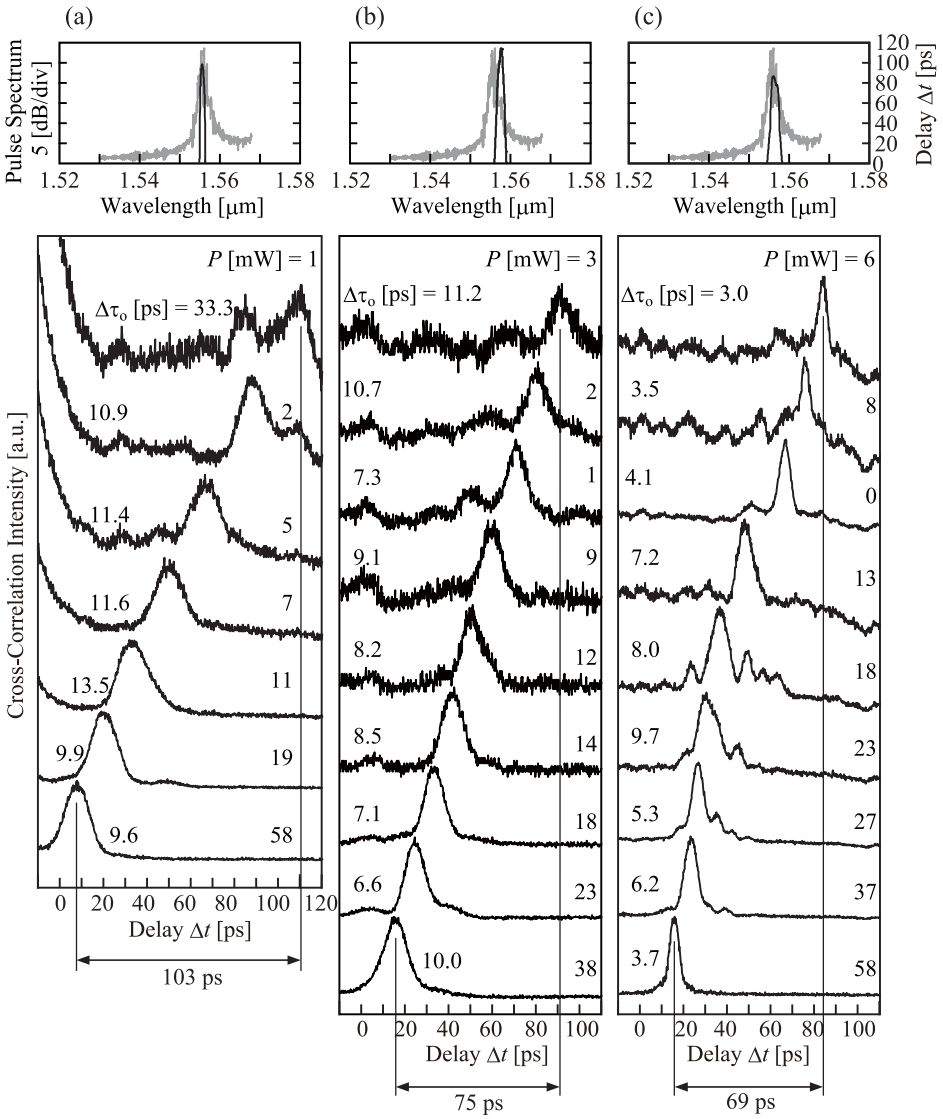

Fig. 7. Delay tuning of different width slow light pulse. Black and gray lines in upper figures show the pulse spectra and slow light spectra, respectively. Lower figures show the normalized cross-correlation trace of output pulse.

V. Device without Airhole Diameter Chirping

Fig. 5(a) and (b) show the transmission and delay spectra of 280 μm long unchirped device adjusted by the post process. The light propagation was observed at λ = 1.53 – 1.57 μm with an intensity dip at λ = 1.556 μm, corresponding to a delay peak up to 115 ps. From the result, ~10 dB loss is roughly estimated for a ~100 ps delay. However, this loss rapidly decreases when the delay and corresponding group index are moderately reduced by adding a chirped structure, as understood from Fig. 4. The maximum group index is as high as 120, and the spectral oscillation is well suppressed compared with our previous result [15]. This is attributed to the post process that optimized the diameter of central airholes $2r_2$ and improved the uniformity of other airholes. The delay at wavelengths shorter and longer than the peak were not the same due to different band slopes, as observed in Fig. 1(b). We also measured the cross-correlation trace of output pulse ($\Delta\lambda_{3dB}$ = 1.0 nm), as shown in Fig. (c) and (d). At three different wavelengths, the pulse delay was coincided with that in the delay spectrum. The pulse was divided into two at the peak wavelength due to large dispersion.

Fig. 6 shows the change of the delay spectrum with the heating. The peak decreased and broadened to the long wavelength side with increasing the heating power *P*. It is the evidence that the folded index chirping is formed. The small spectral oscillation suggests that the index chirping is smooth. As shown in Fig. 7, we then measured the pulse transmission, with the heating. The cross-correlation intensity is normalized in this figure, but it actually decreased with increasing the delay, as understood from the change of the background noise level.

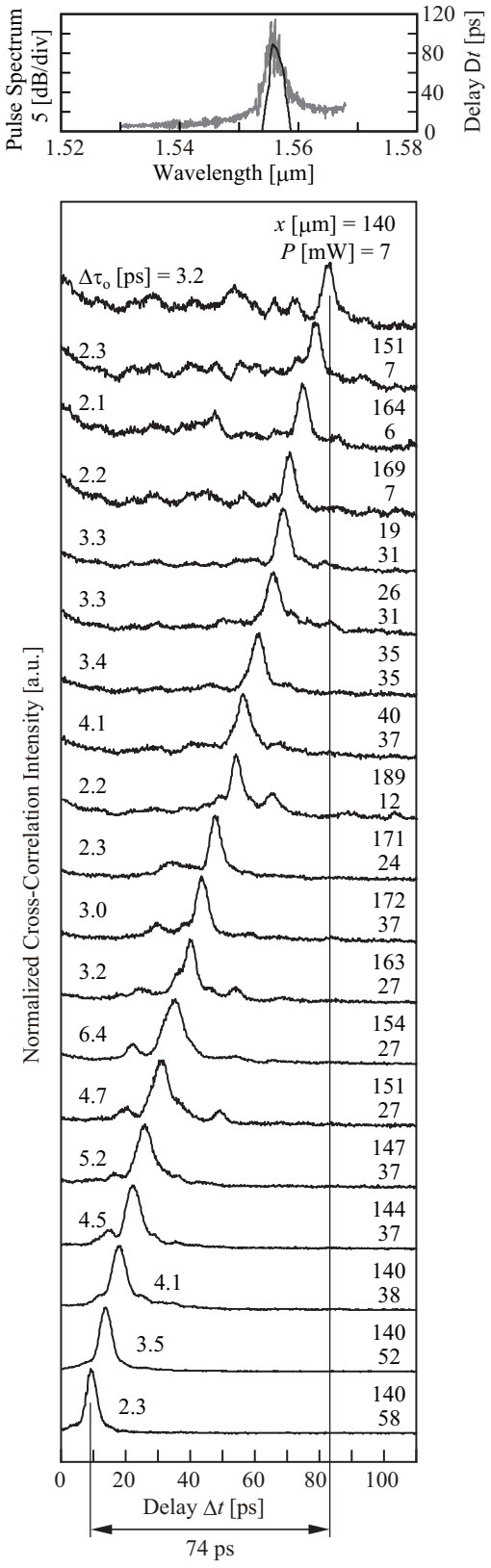

Fig. 8. Delay tuning of slow light pulse when the position of the laser spot and the heating power were simultaneously optimized. Here, x is defined as a distance from the branch.

We set three different pulse widths $\Delta\tau_{ref}$ = 10.2, 9.0, and 3.9 ps by employing different filtering bandwidths $\Delta\lambda_{3dB}$ = 0.68, 0.70, and 1.4 nm (spectral width at –10 dB intensity, λ_{10dB} = 1.2, 1.7, and 2.2 nm), respectively. In general, a narrower spectral width enables a long delay around the peak and gives a wider tuning range. For $\Delta\lambda_{3dB}$ = 0.68 nm in (a), the pulse delay Δt with the weakest heating reached 111 ps, which is almost the same as the peak value in the delay spectrum. As the heating is increased, Δt decreased to 8 ps in the fast light regime. Thus, the tuning range was 103 ps. The average pulse width $\Delta\tau_o$ was 11.4 ps. For $\Delta\lambda_{3dB}$ = 0.70 nm in (b), the pulse shifted while retaining its shape when the center wavelength was set at slightly longer than the peak. Here, the behavior of the pulse shift with P is complicated. For weak heating, the delay peak redshifted and Δt increased up to 91 ps. For stronger heating, the peak further redshifted and broadened, resulting in rapid decrease in Δt up to 16 ps. The tuning range was 75 ps, and average $\Delta\tau_o$ was 8.4 ps. When the pulse was further narrowed, the dispersion became severe. For $\Delta\lambda_{3dB}$ = 1.4 nm, a tuning range of 69 ps was obtained. However, the delay was not able to be controlled continuously at $\Delta t \sim 60$ ps because of the abrupt change of the delay spectrum. Accordingly, the pulse was dispersed or disrupted during tuning.

Then, we finally optimized the center position of the heating, x, simultaneously with P so that the dispersion is minimized, as shown in Fig. 8. The intricate change of x and P is not necessarily based on the simple concept described above. But in any case, we successfully obtained a wide tuning range for narrower pulse; when $\Delta\lambda_{3dB}$ = 1.4 nm ($\Delta\lambda_{10dB}$ = 2.6 nm), a 74 ps delay was obtained with maintaining the output pulse width $\Delta\tau_o$ of 3.4 ps on an average. This indicates a large tunable buffering capacity of 22.

VI. Conclusion

We improved the slow light characteristics and expanded the tuning range of the pulse delay in the SOI photonic crystal coupled waveguide by employing a folded chirp profile. We fabricated the device with the folded chirping of the airhole diameter. Thanks to the large slope folded chirping, the influence of the structural disordering was suppressed. In a 400-μm-long device, a 0.9-ps-wide slow light pulse was delayed for 72 ps, which indicates a buffering capacity of 80 bits. We also fabricated a 280-μm-long unchirped device purely controlled by the thermally induced folded index chirping. The maximum tuning range was 103 ps for a 11.4-ps-wide pulse. By optimizing the heating position, a tuning range of 74 ps was achieved for an average pulse width of 3.4 ps, corresponding to a tunable capacity of 22 bits.

We can expect a nanosecond order delay by prolonging the device to millimeters, further adjusting the structure using the post process, and exploring the mechanism of lowering loss in chirped structures. These values still have much room for improvement toward a practical optical buffer in photonic packet switches. Meanwhile, they are approaching to a level that is applicable to advanced time-domain optical signal

processings such as convolution integrals and phase array antennas. Demonstration of some device applications will be an important next step of the slow light research.

REFERENCES

[1] T. F. Krauss, "Why we need slow light," *Nature Photonics*, vol. 2, pp. 448-450, 2008.

[2] T. Baba, "Slow light in photonic crystals," *Nature Photonics*, vol. 2, pp. 465-473, 2008.

[3] M. Notomi, K. Yamada, A. Shinya, J. Takahashi, C. Takahashi, and I. Yokohama, "Extremely large group velocity dispersion of line-defect waveguides in photonic crystal slabs," *Phys. Rev. Lett.*, vol. 87, pp. 253902, 2001.

[4] Y. A. Vlasov, M. O'Boyle, H. F. Hamann, and S. J. McNab, "Active control of slow light on a chip with photonic crystal waveguides," *Nature*, vol. 438, pp. 65-69, 2005.

[5] H. Gersen, T. J. Karle, R. J. P. Engelen, W. Bogaerts, J. P. Korterik, N. F. van Hulst, N. F., T. F. Krauss, and L. Kuipers, "Real-space observation of ultraslow light in photonic crystal waveguides," *Phys. Rev. Lett.*, vol. 94, pp. 073903, 2005.

[6] M. D. Settle, R. J. P. Engelen, M. Salib, A. Michaeli, L. Kuipers and T. F. Krauss, "Flatband slow light in photonic crystals featuring spatial pulse compression and terahertz bandwidth," *Opt. Express*, vol. 15, pp. 219-226, 2007.

[7] Y. Hamachi, S. Kubo and T. Baba, "Slow light with low dispersion and nonlinear enhancement in a lattice-shifted photonic crystal waveguide," *Opt. Lett.*, vol. 34, no. 7, pp. 1072-1074, 2009.

[8] B. Corcoran, C. Monat, C. Grillet, D. J. Moss, B. J. Eggleton, T. P. White, L. O'Faolain and T. F. Krauss, "Green light emission in silicon through slow-light enhanced third-harmonic generation in photonic-crystal waveguides," *Nature Photonics*, vol. 3, no. 4, pp. 206-210, 2009.

[9] Q. Xu, J. Shakya, and M. Lipson, "Direct measurement of tunable optical delays on chip analogue to electromagnetically induced transparency", *Opt. Express*, vol. 14, no. 14, pp. 6463-6468, 2006.

[10] F. Xia, L. Sekaric, and Y. Vlasov, "Ultracompact optical buffers on a silicon chip," *Nature Photonics*, vol. 1, pp. 65-71, 2007.

[11] F. Morichetti, A. Melloni, C. Ferrari, and M. Martinelli, "Error-free continuously-tunable delay at 10 Gbit/s in a reconfigurable on-chip delay-line", *Opt. Express*, vol. 16, pp. 8395-8405, 2008.

[12] M. Notomi, E. Kuramochi and T. Tanabe, "Large-scale arrays of ultrahigh-Q coupled nanocavities," *Nature Photonics*, vol. 2, pp. 741-747, 2008.

[13] D. Mori and T. Baba, "Dispersion-controlled optical group delay device by chirped photonic crystal waveguides," *Appl. Phys. Lett.*, vol. 85, pp. 1101-1103, 2004.

[14] D. Mori and T. Baba, "Wideband and low dispersion slow light by chirped photonic crystal coupled waveguide," *Opt. Express*, vol. 13, pp. 9398-9408, 2005.

[15] T. Kawasaki, D. Mori and T. Baba, "Experimental observation of slow light in photonic crystal coupled waveguides," *Opt. Express*, vol. 15, pp. 10274-10281, 2007.

[16] T. Baba, T. Kawasaki, H. Sasaki, J. Adachi and D. Mori, "Large delay-bandwidth product and tuning of slow light pulse in photonic crystal coupled waveguide," *Opt. Express*, vol. 16, pp. 9245-9253, 2008.

[17] E. Kuramochi, M. Notomi, S. Hughes, A. Shinya, T. Watanabe and L. Ramunno, "Disorder-induced scattering loss of line-defect waveguides in photonic crystal slabs," *Phys. Rev. B.*, vil. 72, pp. 161318, 2005.

[18] R. J. P. Engelen, D. Mori, T. Baba and L. Kuipers, "Two regimes of slow-light losses revealed by adiabatic reduction of group velocity," *Phys. Rev. Lett.*, vol. 101, pp. 103901, 2008.

Jun Adachi received the B. E. degree from the Department of Electrical and Computer Engineering, Yokohama National University (YNU), Yokohama, Japan, in 2008. He is currently working towards the M. D. degree in photonic crystal slow light buffer at Yokohama National University. Mr. Adachi is a member of the Japan Society of Applied Physics.

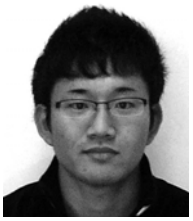

Norihiro Ishikura received the B. E. degree from the Department of Electrical and Computer Engineering, Yokohama National University (YNU), Yokohama, Japan, in 2009. He is currently working towards the M. D. degree in photonic crystal slow light buffer at Yokohama National University. Mr. Ishikura is a member of the Japan Society of Applied Physics.

Hirokazu Sasaki received the B. E. and M. E. degrees from the Department of Electrical and Computer Engineering, Yokohama National University (YNU), Yokohama, Japan, in 2007 and 2009, respectively. During his study, he successfully demonstrated the tunable slow light pulse, for the first time. Currently he is with KDDI Corp.

Toshihiko Baba (M'03) received the Ph. D. Degree from the Division of Electrical and Computer Engineering, Yokohama National University (YNU), Japan, in 1990. During his Ph. D. work, he had been engaged in on-Si waveguides, ARROW waveguides, and 3D photonic integration. From 1991 – 1993, he joined Tokyo Institute of Technology as a research associate. He discussed the spontaneous emission control in VCSELs and achieved the room temperature cw operation in a long wavelength device. He became an associate professor and full professor of YNU in 1994 and 2005, respectively. In these 15 years, he has studied photonic nanostructures such as photonic crystals (PCs), high-index-contrast structures, and Si photonics. He first demonstrated PC waveguides, surface-PC LEDs, and Si photonic wire components. He also achieved the room temperature cw operation in PC nanolasers and microdisk lasers with the strong Purcell effect, record high single-mode power holey VCSEL, negative refractive components for lightwaves, and ultra-compact Si AWG demultiplexer. His recent study is focusing on slow light in PC waveguides towards optical buffering and nonlinear enhancement.

Dr. Baba is a member of the Institute of Electronics, Information and Communication Engineers, the Japan Society of Applied Physics, Optical Society of America, and American Physics Society. He received nine academic awards including JSPS Award in 2005 and LEOS Distinguished Lecturer Award in 2006-2007.